Scientific Bulletin of the
Politehnica University of Timisoara
Transactions on Mechanics
Special issue

2nd Workshop on
Vortex Dominated Flows
Bucharest, Romania
June 30 – July 1, 2006

THREE-DIMENSIONAL SIMULATIONS OF QUANTIZED VORTICES IN ROTATING BOSE-EINSTEIN CONDENSATES

Ionut DANAILA, Assoc. Prof. *
Laboratoire Jacques-Louis Lions
Université Pierre et Marie Curie (Paris 6)

**Corresponding author*: 175 rue du Chevaleret, 75013 Paris, France.
Tel.: (+33) 1 44 27 69 71, Fax: (+33) 1 44 27 72 00, Email: ionut.danaila@upmc.fr

ABSTRACT

Quantized vortices were first predicted and discovered in superfluid ^4He. The first experimental realization in 1995 of a Bose-Einstein condensate (BEC) has opened novel research directions on the properties associated to vortices in a macroscopic system with quantum properties. The reason is that a dilute-gas BEC is a highly controllable system which supports a simple theoretical description. Different methods are experimentally used to generate vortices in a BEC: moving an object (laser beam) through the condensates, rotating the condensate, and, recently, imprinting topological defects by phase-engineering.

In this paper, we review our recent numerical results on the vortex structure of rotating BECs. This work was motivated by recent experimental achievements by the École Normale Supérieure (ENS) group. Using real experimental parameters in a three-dimensional (3D) numerical simulation of fast rotating BECs is a challenging proposition since the capture of the large number of vortices in the system requires high grid-resolution and accurate numerical methods.

Our numerical results are obtained by propagating the three-dimensional Gross-Pitaevskii equation in imaginary time. A high order (compact) finite difference method is used for the spatial discretization. We characterize several equilibrium vortex configurations obtained for different trapping potentials. Numerical data are compared to available experimental and theoretical results and a remarkably good qualitative and quantitative agreement is found.

KEYWORDS

Quantized vortices, Gross Pitaevskii equation, Scrödinger equation, Bose Enstein condensate, Abrikosov lattice, imaginary time, finite differences, compact schemes.

NOMENCLATURE

$\psi = \sqrt{\rho} e^{i\theta}$	[-]	macroscopic wave function
u	[-]	dimensionless wave function
$\rho = \lvert u \rvert^2$	[-]	atomic density
m	[-]	atomic mass of the gas
a_s	[-]	scattering length
ξ	[-]	healing length
μ	[-]	chemical potential
Ω	[-]	angular velocity
x, y, z	[-]	Cartesian coordinates in the rotating frame
$r = \sqrt{x^2 + y^2}$	[-]	distance to the center
$\omega_{x,y,z}$ $\omega_\perp$	[-]	trapping frequencies
r_v	[-]	vortex core radius
b_v	[-]	inter-vortex spacing
$h,\ \hbar = h/2\pi$	[-]	Plank's constant
κ_B	[-]	Boltzmann's constant

ABBREVIATIONS

3D	three-dimensional
BEC	Bose-Einstein condensate
GP	Gross-Pitaevskii
TF	Thomas-Fermi

1. INTRODUCTION

Bose Einstein condensates (BEC) owe their name to the prediction of Bose and Einstein in 1925: for a gas of non interacting particles at very low temperature, a macroscopic fraction of the gas is in the state of lowest energy, that is condensed. As a consequence, the atoms in the condensate oscillate following the same complex wave function ψ. The first experimental realization of atomic BEC in 1995 was awarded the Nobel Prize in 2001, the laureates being E. A. Cornell (University of Colorado), W. Ketterle (MIT) and Carl E. Wieman (University of Colorado) [1]. Since then, a lot of properties of these systems have been studied both experimentally and theoretically (see, for instance, [2]).

In recent years, several experimental studies provided evidence for the existence of quantized vortices in rotating Bose-Einstein condensates [3, 8, 9]. The condensate is typically confined by a magnetic potential and set into rotation using a laser beam, which can be assimilated to a spoon stirring a cup of tea (see Fig. 1). The number and shape of vortices depend on the rotational frequency and the geometry of the trap. We consider here elongated traps resulting in cigar-shape condensates, corresponding to experiments performed by the École Normale Supérieure (ENS) group [2]. Typical size of the condensate is 100 μm for the length and 10 μm for the diameter.

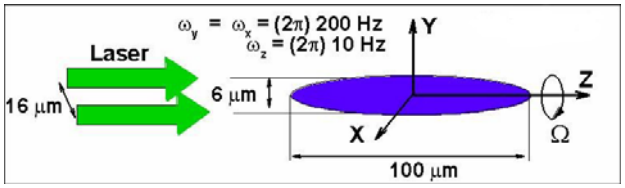

Figure 1. Sketch of a rotating cigar-shape condensate corresponding to experiments described in Ref. [2].

Quantized vortices start to nucleate in the condensate when the rotation frequency Ω exceeds a critical value Ω_c. If the condensate is described by the macroscopic wave function

$$\psi = \sqrt{\rho(x,y,z)}\ \exp(i\ \theta(x,y,z)), \tag{1}$$

where ρ is the local density and θ the phase, a quantized vortex is a topological defect of ψ. In other words, $\rho = 0$ in the core of the vortex (there are no atoms) and around the vortex there exists a frictionless superfluid flow with a discontinuous phase field. Therefore, if the local velocity in a point where the density is non-zero is defined as

$$\mathbf{v} = \frac{h}{2\pi\ m}\nabla\theta = \frac{\hbar}{m}\nabla\theta, \tag{2}$$

the circulation around a vortex will be quantized (Fig. 2)

$$\Gamma = \oint \mathbf{v}\,.\,\mathbf{dl} = n\frac{h}{m} \tag{3}$$

where h is the Planck's constant, m the atomic mass and n an integer. The quantification of the circulation is a striking feature of superfluid vortices compared to vortices in classical fluids.

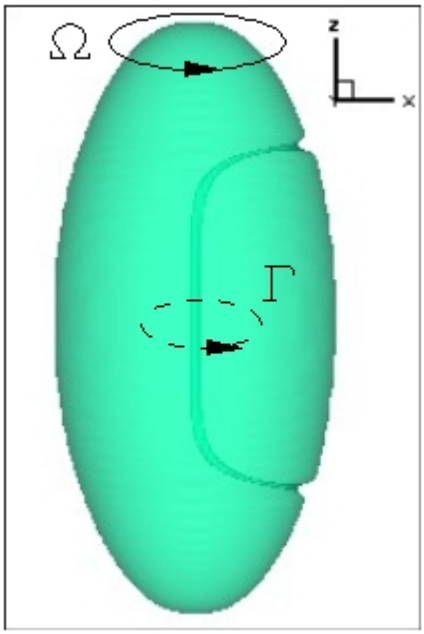

Figure 2. Numerical simulation of a singly quantized vortex in a cigar-shape condensate. Identification by means of iso-surface of low density $\rho = |\psi|^2$.

This description suggests a simple method for the identification of vortices in numerical simulations by plotting iso-surfaces of low density $\rho = |\psi|^2$, as shown in Fig. 2 for a singly quantized vortex (n=1). It is interesting to note in passing that in classical fluid dynamics there are still controversial debates on the general definition of a vortex.

For the trapping potentials considered in the following, only singly quantized vortices are obtained. When increasing $\Omega > \Omega_c$, more and more vortices appear and arrange themselves into a

regular triangular (Abrikosov) lattice, as will be seen below.

In this paper, we review our recent numerical results, most of them being contained in [4]. A high order finite difference method is proposed to numerically investigate the three-dimensional shape of equilibrium vortex configurations in a prolate (cigar-shape) rotating condensate. Our aim is to understand the various vortex configurations observed in experiments with different trapping potentials. This is not without its challenges, since the description of a condensate with a large number of vortices (exceeding 100) requires very high spatial resolution and accurate integration schemes. Computations become very expensive at high rotation frequencies, which explains why such 3D simulations are not, to the author's knowledge, currently available in the open literature.

2. MATHEMATICAL MODEL

We consider a pure BEC of N atoms confined in a trapping potential V_{trap} rotating along the z axis at angular velocity Ω. The energy of the system in the rotating frame is described by the Gross-Pitaevskii (GP) functional:

$$\mathrm{E}_{3D}(\psi) = \iiint_D \frac{\hbar^2}{2m}|\nabla\psi|^2 + \mathrm{V}_{\mathrm{trap}}|\psi|^2 + \frac{Ng_{3D}}{2}|\psi|^4 + \hbar\Omega.(i\psi, \nabla\psi \times \mathbf{x}). \quad (4)$$

The interaction coefficient is defined as $g_{3D} = 4\pi\,\hbar^2\,a_s/m$, where a_s is the scattering length. The wave function is normalized to unity i.e. $\iiint_D |\psi|^2 = 1$. The trapping potential has usually the (harmonic) form:

$$V_{trap}(x,y,z) = \frac{1}{2}m\left(\omega_x^2x^2 + \omega_y^2y^2 + \omega_z^2z^2\right), \quad (5)$$

with $\omega_{x,y,z}$ the trap frequencies along each spatial direction.

For numerical purposes, it is convenient to use the scaling introduced in [5]: $\mathbf{r} = \mathbf{x}/R$, $u(\mathbf{r}) = R^{3/2}\psi(\mathbf{x})$, where $R = d/\sqrt{\varepsilon}$ and

$$d = \left(\frac{\hbar}{m\omega_x}\right)^{1/2}, \varepsilon = \left(\frac{d}{8\pi Na_s}\right)^{2/5}, \tilde{\Omega} = \frac{\Omega}{\varepsilon\omega_x}. \quad (6)$$

The 3D dimensionless energy becomes

$$E(u) = H(u) - \tilde{\Omega}\,L_z(u), \quad (7)$$

where H is the hamiltonian

$$H(u) = \iiint_D \frac{1}{2}|\nabla u|^2 + \frac{|u|^2}{2\varepsilon^2}\mathrm{V(r)} + \frac{1}{4\varepsilon^2}|u|^4, \quad (8)$$

V the dimensionless potential and L_z the angular momentum

$$L_z(u) = \iiint_D \bar{u}(y\partial_x - x\partial_y u). \quad (9)$$

The equilibrium of the system corresponds to minima of the Gross-Pitaevskii energy.

3. NUMERICAL MODEL

We compute critical points of $E(u)$ by solving the norm-preserving imaginary time propagation of the corresponding equation:

$$\frac{\partial u}{\partial t} - \frac{1}{2}\nabla^2 u + i(\tilde{\Omega}\times\mathbf{r}).\nabla u = -\frac{u}{2\varepsilon^2}(\mathrm{V} + |u|^2) + \mu_\varepsilon u\ , \quad (10)$$

where μ_ε is the Lagrange multiplier for the constraint $\iiint_D |u|^2 = 1$ and $u = 0$ on ∂D. Here, D is a rectangular domain containing the condensate.

A hybrid 3 steps Runge-Kutta-Crank-Nicolson scheme [6] is used to advance the equation in time:

$$\frac{u_{l+1} - u_l}{\delta t} = a_l F_l + b_l F_{l-1} + c_l \nabla^2\left(\frac{u_{l+1} + u_l}{2}\right), \quad (11)$$

where F contains the remaining non-linear terms. The corresponding constants for every step $l = 1,2,3$ are:

$$\begin{aligned} &\mathrm{a}_1 = 8/15, \mathrm{a}_2 = 5/12, \quad \mathrm{a}_3 = 3/4, \\ &\mathrm{b}_1 = 0, \quad \mathrm{b}_2 = -17/60, \quad \mathrm{b}_3 = -5/12, \\ &\mathrm{c}_1 = 8/15, \mathrm{c}_2 = 2/15, \quad \mathrm{c}_3 = 1/3. \end{aligned} \quad (12)$$

The resulting semi-implicit scheme is second order time accurate and allows reasonably large time steps, making it appropriate for long time integration. The large sparse matrix linear systems

resulting from the implicit terms are solved by an alternating direction implicit (ADI) factorization technique.

For the spatial discretization we use finite differences on a Cartesian uniform mesh. To accurately resolve sharp gradients of the variable in presence of vortices, low numerical dissipation and very accurate schemes are required for the spatial derivatives. A sixth-order compact finite difference scheme [7] with spectral-like resolution was chosen to this end. For example, the first and second derivatives at the grid point *i*, far from the boundaries, are written as :

$$\frac{1}{3}u'_{i-1} + u'_i + \frac{1}{3}u'_{i+1} = \frac{14}{9}\frac{u_{i+1}-u_{i-1}}{2\delta x} + \frac{1}{9}\frac{u_{i+2}-u_{i-2}}{4\delta x}, \quad (13)$$

$$\frac{2}{11}u''_{i-1} + u''_i + \frac{2}{11}u''_{i+1} = \frac{12}{11}\frac{u_{i+1}-2u_i+u_{i-1}}{\delta x^2} + \frac{3}{11}\frac{u_{i+2}-2u_i+u_{i-2}}{4\delta x^2}, \quad (14)$$

where δx is the step of the space discretization. The values of the derivatives at all the grid points are computed by solving a tridiagonal matrix linear system, which provides spectral-like behavior of the finite difference scheme.

The size of the computational domain is estimated by starting from the theoretical Thomas-Fermi (TF) density distribution law:

$$\rho_{\mathrm{TF}} = \frac{m}{4\pi\hbar^2 a_s}\left(\mu - V_{trap}(r,z) + \frac{1}{2}m\Omega^2 r^2\right) \quad (15)$$

where $r = \sqrt{x^2+y^2}$ and μ is the chemical potential given by the constraint $\iiint_D \rho_{TF}(r,z) = 1$. The maximum transverse radius $R_\perp$ and longitudinal half-length R_z can be then calculated from Eq. (15) in order to estimate the dimensions of the rectangular computational domain. For high Ω (when the condensate is nearly spherical and more than 100 vortices are present), up to $240\times240\times240$ grid points are used to compute equilibrium states.

It is worth at this point to describe how the condensate evolves in the "imaginary" time (i.e. how it relaxes to an equilibrium state). A typical simulation starts either from an initial condition given by the steady-state TF density distribution (15) - no vortices in the condensate -, or from an artificial field obtained by superimposing to the steady-state a simplified model for vortices. When solution branches are followed, the converged field for lower Ω is used as initial condition.

When suddenly increasing Ω, new vortices are generated at the border of the condensate and enter the condensate. In the first stages of the computation, 3D vortex lines are strongly distorted, giving a *spaghetti* image of the lattice (see Fig.3).

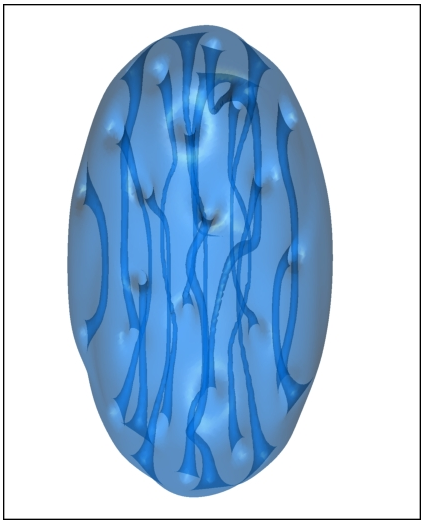

Figure 3. Spaghetti-like vortex structure in a condensate evolving in the imaginary time before convergence to an equilibrium state.

Close to equilibrium, vortices become straight in their central part and arrange themselves in a more and more regular lattice (Fig. 4). Convergence is particularly slow at the end of the computation when the position and shape of vortices evolve very slowly. Convergence is considered when the energy remains constant (relative fluctuations less than 10^{-6}) for a relatively long time to be sure that a stable state was obtained. The convergence time is longer for high values of the rotation frequency.

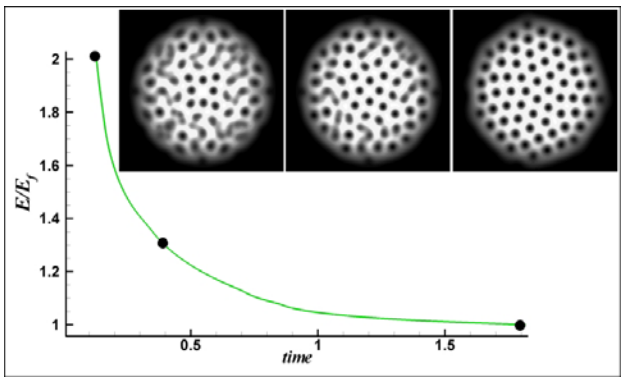

Figure 4. Example of energy decrease during the propagation of 3D Gross-Pitaevskii equation in imaginary time. Energy is normalized by the equilibrium (final) value E_f. Inserts show iso-contours of the integrated (along z) density corresponding to three successive time instants represented on the energy curve.

4. DESCRIPTION OF THE RESULTS

We describe in detail the three dimensional structure of vortices for different trapping potentials used in experiments.

4.1. Harmonic trapping potential

In experiments, the condensate is typically confined by the harmonic (quadratic) potential given by Eq. (5). The values of constants in (10) are set to

$$\varepsilon = 0.02,\ \ \alpha = \frac{\omega_y}{\omega_x} = 1.06,\ \ \beta = \frac{\omega_z}{\omega_x} = 0.067,$$

corresponding to the experiments of the ENS group. The condensate is made of ^{87}Rb and has the following physical parameters:

$$m = 1.445 \cdot 10^{-25}\ \text{kg},\ \ a_s = 5.8 \cdot 10^{-9}\ \text{m},$$

$$N = 1.4 \cdot 10^{5},\ \ \omega_x = 1094\ \text{s}^{-1}.$$

The angular frequency Ω is varied from 0 to the maximum value of $0.9\omega_x$.

This type of potential was used to experimentally study single vortex lines in a cigar-shape (or prolate) condensate [8]. Experimental evidence was provided to prove that the vortex line is not straight along the axis of rotation, but bending. The vortex displays therefore a U shape. More complicated configurations (S vortices) were also observed in experiments.

Our numerical simulations reproduce remarkably well these vortex shapes (Fig. 5). The U vortex (see Fig. 5a) was numerically obtained by starting the simulation from an initial condition containing a straight vortex away from the z axis. For a relatively large value of the rotation frequency, the final steady state (i.e. the local minimum of the GP energy) displays a planar U shape with a straight central part on the z axis and an outer part reaching the condensate boundary perpendicularly.

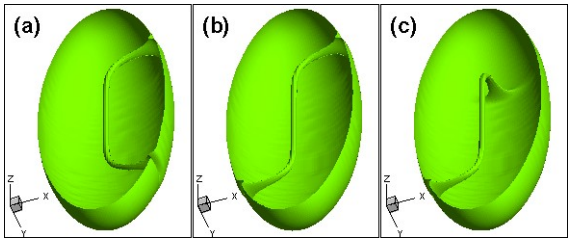

Figure 5. Single vortex lines in a prolate (cigar-shape) rotating condensate with harmonic trapping potential: U vortex (a), planar S vortex (b) and non-planar S vortex (c).

The U vortex exists for the range $0.42 \le \Omega/\omega_x \le 0.86$. When varying Ω at the lower bound, the U vortex disappears and a vortex-free configuration is obtained, while at the higher bound the U vortex degenerates in a three-vortex configuration.

Planar S vortices (see Fig. 5b) were numerically obtained from artificial generated initial conditions containing such a vortex. We checked that the final steady state for a given Ω is always the same (different initial planar S shapes evolved to the same final configuration). The S vortex exists for all values of Ω - they are only local minima of the GP energy. We also obtained S vortices with the bent arms rotated by 90 degrees (see Fig. 5c). We could check that non planar S configurations with an angle between the branches different from 90 degrees, do not exist. For a given Ω, the three configurations are topologically equivalent by a z-rotation of the bent arms of the vortices.

The two branches of solutions (U and S) were followed by continuation and the energy diagram is plotted in Fig. 6. It is interesting to note that at Ω_c, when the U vortex appears, the energy of the U vortex is bigger than the energy of the vortex free solution (we have set to zero the energy of the vortex free solution).

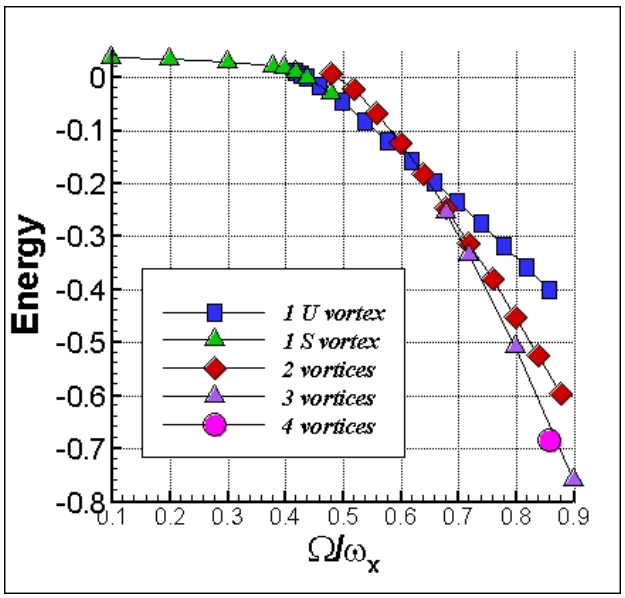

Figure 6. Harmonic trapping potential: energy (in units of $\hbar\omega_x$) for the single vortex configurations.

4.2. "Quartic plus harmonic" trapping potential

The harmonic trapping potential allows for rotation frequencies lower than ω_x; for $\Omega = \omega_x$ the centrifugal force compensates the trapping force and the confinement of the atoms vanishes. The fast rotation regime, corresponding to $\Omega \cong \omega_x$, is the focus of a lot of attention since new physical phenomena are expected.

The experimental approach to reach the fast rotation regime explored by the ENS group [9] consists in modifying the quadratic (harmonic) trapping potential by superimposing a blue detuned laser beam to the magnetic trap holding the atoms. The resulting *harmonic-plus-Gaussian* potential removes the singularity at the limit $\Omega = \omega_x$ and allows to reach rotation rates up to $\Omega = 1.05\omega_x$.

The trapping potential becomes

$$V_{trap}(r,z) = V_h(r,z) + U(r), \tag{16}$$

where

$$V_h(r,z) = \frac{1}{2}m\left(\left(\omega_\perp^0\right)^2 r^2 + \omega_z^2 z^2\right), \tag{17}$$

$$U(r) = U_0 \exp(-2r^2/w^2).$$

The trapping frequencies are $\omega_\perp^0 = 2\pi \cdot 75.5\,\text{Hz}$ and $\omega_z = 2\pi \cdot 11$ Hz, resulting in a cigar-shape condensate. The laser waist is $w = 25\ \mu\text{m}$ and the amplitude of the laser beam is $U_0 = \kappa_B \cdot 90\,\text{nK}$, where κ_B is the Boltzman's constant.

For r/w sufficiently small, the potential V_{trap} can be approximated by:

$$V_1 = \left[\frac{1}{2}m\left(\omega_\perp^0\right)^2 - \frac{2U_0}{w^2}\right]r^2 + \frac{2U_0}{w^4}r^4 + \frac{1}{2}m\omega_z^2 z^2. \tag{18}$$

For this *quadratic-plus-quartic* potential, the equivalent transverse trapping frequency is decreased to $\omega_\perp = 2\pi \cdot 65.6$ Hz. Since the amplitude U_0 of the laser beam is low in experiments, the quadratic part of the potential V_1 remains positive (repulsive interactions) and the quartic part is very small.

The numerical evolution of the 3D structure of the condensate with increasing Ω can be seen in Fig. 7. The simulations offer a detailed 3D picture of vortex configurations that is not available from experiments and 2D simulations. In particular, the vortex merging leading to the formation of the central hole (giant vortex) in a condensate is proved to be highly three-dimensional and is clearly observed, which is not the case in experiments. The giant vortex can be regarded as the region containing singly quantized vortices with such low density that they are discernible only by the phase defects.

Our simulations also provide quantitative information on the characteristics of the vortex lattice, namely the inter-vortex spacing b_v and the vortex core size r_v. We find that r_v scales with the healing length $\xi = \sqrt{8\pi a_s \rho}$, as is usually assumed in theoretical studies. The variation of b_v with the distance to the center of the condensate describes the vortex lattice inhomogeneities; a remarkably good agreement is found with the theoretical findings of Sheehy and Radzihovsky [10] (see Fig. 8).

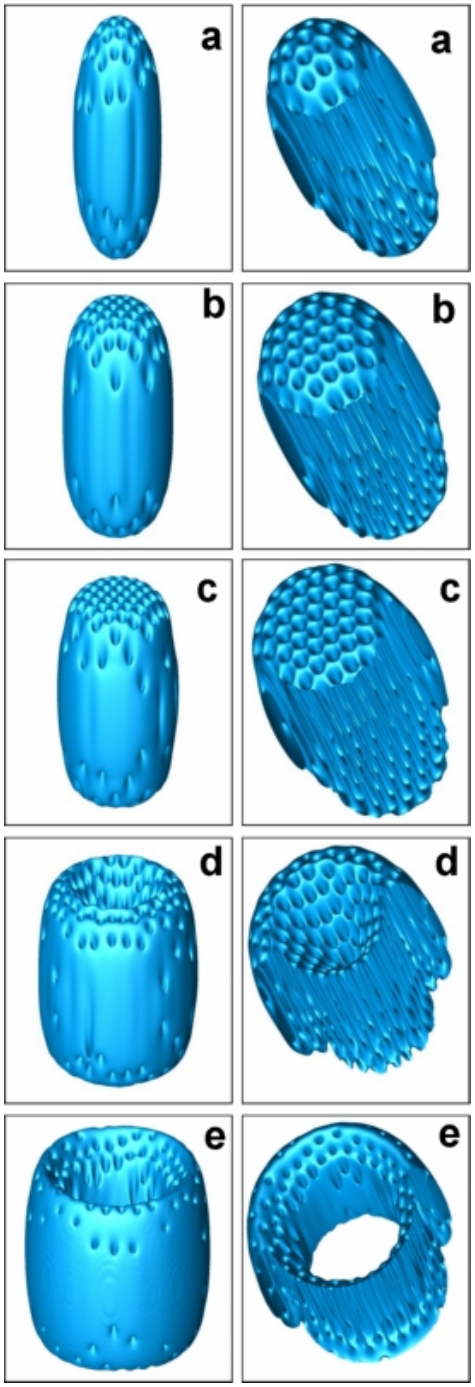

Figure 7. Numerically generated condensates obtained using a quadratic+quartic trapping potential with the parameters corresponding to experiments of [9]. Each column corresponds to a value of the rotation frequency - from top to bottom: $\Omega/2\pi = 60,64,66,70.4,73$ (respectively, $\Omega/\omega_\perp = 0.92,0.98,1.01,1.08,1.11$). Three-dimensional views of the vortex lattice identified by means of iso-surfaces of low atomic-density.

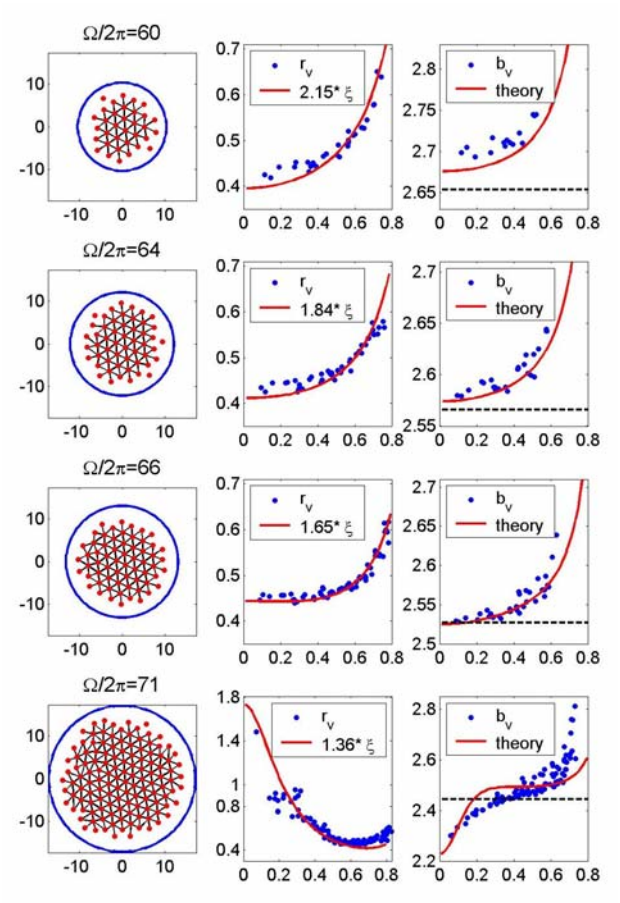

Figure 8. Harmonic plus quartic potential: vortex lattice and variation of vortex core radius r_v and inter-vortex spacing b_v (values in μm) as functions of the non-dimensional radius $r/R_\perp$. For each plot, the value of the rotation frequency ($\Omega/2\pi$) is indicated. In plots displaying r_v, solid line represents the variation of the healing length ξ, scaled by a constant indicated in the legend. Variation of b_v is compared to theory prediction [10] (solid line) and the estimation assuming a uniform (rigid-body) vortex distribution (dashed line).

4.3. "Quartic minus harmonic" trapping potential

It is interesting to note that a stronger amplitude U_0 in Eq. (18) could generate a *quartic-minus-harmonic* potential (the interactions in the condensate becomes repulsive, instead of attractive as previously). We numerically found that this type of potential allows to obtain a giant vortex in the condensate at lower rotation frequencies than for the "quartic-plus-harmonic" potential. Indeed, Fig. 9 shows condensates with a giant vortex starting from

$\Omega/\omega_\perp \geq 0.12$. As Ω is increased, singly quantized vortices are nucleated on a circle around the central hole. To our knowledge, this transition (which is similar to the case of the rotating bucket experiment for helium) has not been studied in BEC.

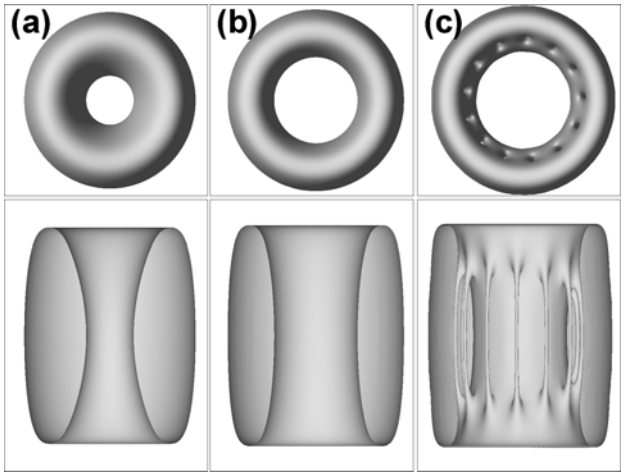

Figure 9. Quartic-minus-harmonic trapping potential: top and side view of the condensate for $\Omega/\omega_\perp = 0.12$ (a), 0.2 (b) and 0.3 (c).

4.4. "Harmonic plus optical lattice" trapping potential

We finally present a sample of recent numerical simulations corresponding to a rotating BEC in an optical lattice, described by a trapping potential of the form:

$$V_{trap}(r,z) = V_h(r,z) + U_s \cdot \sin^2(\pi \frac{z}{z_0}). \qquad (19)$$

Intriguing vortex arrangements (see Fig. 10) are obtained for the bands of the optical lattice when the amplitude U_s is increased. Since experimental data are not yet available for such rotating configuration, our numerical simulations contribute to the theoretical description of interesting phenomena in rotating BECs. This work is in progress.

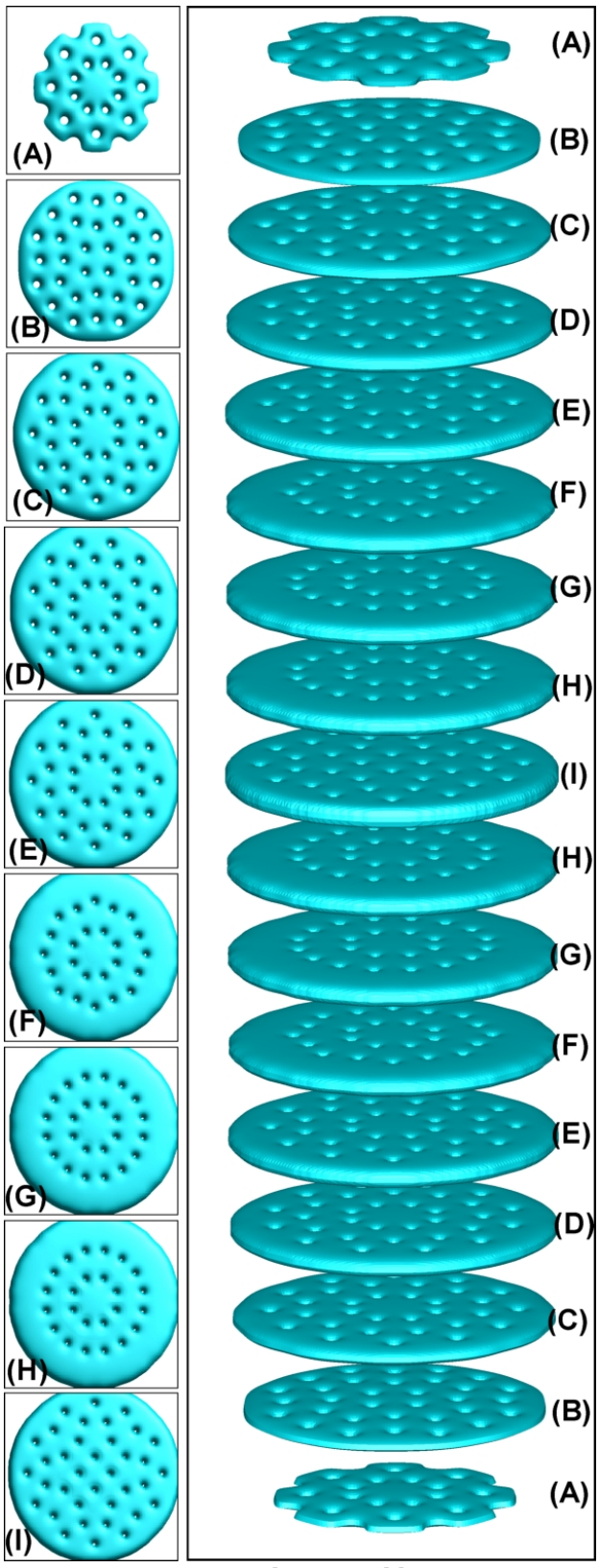

Figure 10. Quartic--plus-optical lattice trapping potential: view of the vortex arrangements for the first 9 individual sites (the condensate is symmetrical with respect to the central plane).

5. CONCLUSION AND FUTURE WORK

We have studied the vortex structure of equilibrium states of a rotating BEC by numerically propagating the Gross-Pitaevskii equation in imaginary time. The spectral-like finite difference scheme proved to be very effective in accurately capturing the three-dimensional structure of vortices. Our simulations offer a detailed 3D picture of vortex configurations that is not available from experiments. Remarkably qualitative and quantitative agreement with available experimental and theoretical results is obtained when using real, experimental parameters, for the simulation.

Future developments of the numerical system are aimed at simulating the real-time dynamics of the condensate (solving the non-linear Schrödinger equation in 3D).

REFERENCES

1. http://nobelprize.org/physics/laureates/2001/
2. http://www.lkb.ens.fr/recherche/atfroids/
3. M. R. Matthews, B. P. Anderson, P. C. Haljan, D. S. Hall, C. E. Wieman, and E. A. Cornell, Phys. Rev. Lett., 83, 2498 (1999).
   J. R. Abo-Shaeer , C. Raman, J. M. Vogels and W. Ketterle, Science , 292, 476 (2001).
   P. C. Haljan, I. Coddington, P. Engels, and E. A. Cornell, Phys. Rev. Lett., 87, 210403 (2001).
4. I. Danaila, *Three-dimensional vortex structure of a fast rotating Bose-Einstein condensate with harmonic-plus-quartic confinement*, Phys. Rev A, 72, 013605 (2005).
   L.-C. Crasovan, V. M. Pérez-García, I. Danaila, D. Mihalache and L. Torner, *Three-dimensional parallel vortex rings in Bose-Einstein condensates*, Phys. Rev A, 70, 033605, (2004).
   A. Aftalion and I. Danaila, *Giant vortices in combined harmonic and quartic traps*, Phys. Rev A, 69, 033608 (2004).
   A. Aftalion and I. Danaila, *Three-dimensional vortex configurations in a rotating Bose Einstein condensate*, Phys. Rev A, 68, 023603 (2003).
5. A. Aftalion and T. Riviere, Phys. Rev. A, 64, 043611 (2001).
6. P. Orlandi, *Fluid Flow Phenomena*, Kluwer Academic Publishers (1999)
7. S. K. Lele, J. Comp. Physics, 103, 16 (1992).
8. K. Madison, F. Chevy, V. Bretin and J. Dalibard, Phys. Rev. Lett., 84, 806 (2000).
   K. Madison, F. Chevy, W. Wohlleben and J. Dalibard, J. Mod. Opt., 47, 2715 (2000).
   C. Raman, J. R. Abo-Shaeer, J. M. Vogels, K. Xu, and W. Ketterle, Phys. Rev. Lett., 87, 210402 (2001).
   P. Rosenbuch, V. Bretin and J. Dalibard, Phys. Rev. Lett., 89, 200403 (2002).
9. V. Bretin, S. Stock, Y. Seurin, and J. Dalibard, Phys. Rev. Lett., 92, 050403 (2004).
   S. Stock, V. Bretin, F. Chevy, and J. Dalibard, Europhys. Lett., 65, 594 (2004).
10. D. E. Sheehy and L. Radzihovsky, Phys. Rev. A , 70, 063620 (2004).